RSC Advances

PAPER

View Article Online
View Journal | View Issue

Cite this: *RSC Adv.*, 2017, **7**, 31549

Preparation and adsorption behaviors of sodium alginate-based adsorbent-immobilized β-cyclodextrin and graphene oxide

Yanchen Wu,† Houjuan Qi,† Cai Shi, Rongxiu Ma, Shouxin Liu and Zhanhua Huang *

Received 24th February 2017
Accepted 25th May 2017

DOI: 10.1039/c7ra02313h

rsc.li/rsc-advances

Highly water soluble graphene oxide (GO) was synthesized *via* a modified Hummers method. A sodium alginate (SA)-based adsorbent-immobilized β-cyclodextrin (β-CD) and GO gel (SCGG) with excellent regeneration ability were prepared. The adsorptive properties of methylene blue (MB) on the SCGG adsorbent were studied. The results showed that when the dosage of the adsorbent was 1.0 g, pH of the solution was 7, temperature was 35 °C, initial concentration of MB was 50 mg L^{-1}, and adsorption time was 180 min, the removal rate of MB was 84.98% and the adsorption capacity was 133.24 mg g^{-1}. The isotherms and kinetics of adsorption were investigated to reveal that the equilibrium adsorption and kinetics were well-described by the Freundlich model and pseudo-second-order kinetics, respectively. The thermodynamic parameters showed that the adsorption process was spontaneous and endothermic in nature. The mechanical property of the SCGG was improved by the addition of GO. The regeneration removal rate of MB was more than 82% after six recycles.

1. Introduction

As is well-known, dyes are widely used in the textile, paper-making, printing, and other industries. Dyes offer convenience to consumers; however, the use of dyes can cause serious harm to the environment due to the indiscriminate discharge of dye wastewater,[1,2] and the deterioration of the environment will affect the human health. How to control the content of dyes in wastewater is a matter of great concern among researchers.[3] Many physical and chemical methods such as adsorption, physical precipitation and flocculation, coagulation, chemical oxidation and reduction, biological treatment, and photocatalytic degradation[4] have been used to remove dyes from wastewater. Among these, adsorption has been developed to deal with dye wastewater problem because this method is faster, cost-effective, and environmentally friendly; furthermore, the design and operation of adsorption process is comparatively easier and it does not result in secondary pollution. The MB dye is a heteroaromatic compound that is used in industrial applications, and it can affect the quality of water. Various adsorbents, such as rice husk,[5] garlic peel,[6] conducing polymers,[7] carbon nanotubes,[8] bamboo activated carbon,[9] cedar sawdust, and crushed brick,[10] have been used for the adsorption of MB. However, some of these adsorbents show limitations in terms of recycling; therefore, an adsorbent with good adsorption capacity and regeneration performance is highly desirable.

A number of adsorbents based on biomass resources have been researched.[11–14] Among these, the SA-based adsorbent is particularly interesting. SA was derived from brown algae and bacterial biosynthesis. It comprises sequences of M (M-blocks) and G (G-blocks) residues interspersed with MG sequences (MG-blocks).[15] SA is biodegradable, biocompatible, renewable, and nontoxic. The guluronic acid of SA can be cross-linked *via* divalent or trivalent cations (such as Ca^{2+}) to obtain an egg-box structure,[16,17] forming a gel. However, the mechanical property of the gel obtained from SA was poor, which limits its regeneration. In order to improve the mechanical property of SA gel, some researchers have explored. Jie *et al.* prepared a carboxyl multi-walled carbon nanotube/calcium alginate composite membrane, and the results showed that the tensile strength of the membrane was improved.[18] Chang *et al.* fabricated hydrogels by blending cellulose and SA solution for the improvement of the mechanical property.[19] GO was also used to enhance the mechanical property *via* a wet spinning method.[20] GO is oxygenated derivative of graphene and possess many excellent properties. GO surfaces and edges contain rich oxygen-containing functional groups including the carboxyl, hydroxyl, and epoxy groups. Moreover, GO exhibits good hydrophilicity and dispersion due to these oxygen-containing functional groups.[21] The large specific surface area and rich oxygen-containing functional groups of GO can provide abundant sites for adsorption. Moreover, when GO is used as a filler, its unique mechanical property can enhance the strength of the material. The outer rim of β-CD is hydrophilic and its inner

Key Laboratory of Bio-based Material Science and Technology of the Ministry of Education, Northeast Forestry University, Harbin 150040, China. E-mail: nefuhzh@nefu.edu.cn

† Co-first authors.

cavity is hydrophobic. Moreover, β-CD possesses a special structure and rich functional groups and can increase the number of oxygen-containing functional groups and adsorption active sites. In addition, β-CD can improve the dispersion of gel balls.

The objective of this study was to obtain a high mechanical property SA-based adsorbent with excellent adsorption and regeneration ability. To improve the mechanical property and the dispersion of the gel beads, GO and β-CD were immobilized on an SA matrix. SCGG was prepared *via* an ion exchange method with SA, GO, and β-CD. To explore the potential application of SCGG in dye removal, MB dye was chosen to test the adsorption behaviors of SCGG. The adsorption isotherms, adsorption kinetics, and thermodynamic performance were studied *via* batch experiments. This study can provide methods for the development of high-performance biological adsorbents. The method for the preparation of the SCGG adsorbent was simple. Furthermore, SCGG possesses good adsorption properties such as shorter equilibrium time, faster adsorption rate, and higher adsorption capacity. Moreover, the mechanical properties of SCGG were improved, and the regeneration ability of SCGG reached at least 6 times due to the addition of GO.

2. Materials and methods

2.1. Materials

Graphite with an average particle size of 30 μm was purchased from Sinopharm Chemical Reagent Co., Ltd. (Shanghai, China). MB cationic dye was obtained from YongDa Chemical Reagent Co., Ltd. (Tianjin, China). SA biopolymer with a viscosity of 1.05–1.15 Pa s was obtained from GuangFu Fine Chemical Research Institute (Tianjin, China). β-CD was purchased from Kermel Chemical Reagent Co., Ltd. (Tianjin, China). All other reagents used were of analytical grade or better and used as received. Herein, 0.1 M NaOH and 0.1 M HCl were used to adjust the pH of the solutions. Deionized water was used to prepare all the dye solutions.

2.2. Preparation of GO

GO was synthesized from natural graphite powder *via* a modified Hummers method.[22,23] In a typical procedure, graphite powder was placed in an 80 °C solution of concentrated H_2SO_4 with $K_2S_2O_8$ and P_2O_5 for 5 h. The mixture was washed with deionized water to remove the residual acid, and the mixture was filtered and dried. The obtained powder was oxidized *via* the Hummers method.[24] The obtained powder was placed in H_2SO_4 (98%, 60 mL) in a round-bottom flask under the stirring condition. Then, $KMnO_4$ was added while the temperature of the mixture was maintained below 5 °C. After this, the temperature was increased to 35 °C for 2 h; then, the mixture was diluted with de-ionized water (92 mL), and the temperature was increased to 70 °C for 0.5 h. After this, deionized water (100 mL) and H_2O_2 (20 mL) were added to the mixture, and the mixture was filtered and washed with HCl aqueous and deionized water to remove metal ions and acid. The resulting filter cake was purified *via* dialysis to remove the remaining metal species. Finally, the suspension was ultrasonically treated for 2 h and centrifuged to remove the unexfoliated GO particles. The GO suspension was thus obtained.

2.3. Preparation of SCGG

The GO suspension was diluted using 100 mL deionized water *via* ultrasonic dispersion for 2 h. SA and β-CD were added to the above mentioned solution with the mass ratio of 1 : 1. The mixed solution was continuously stirred until a homogeneous solution was formed. Then, the homogeneous solution was left undisturbed to remove the air bubbles. After this, the homogeneous solution was dropped into the 5 wt% solution of $CaCl_2$ using a syringe. The beads were left in the $CaCl_2$ solution for 12 h and washed three times with deionized water to obtain the stable gel beads (SCGG).

2.4. Adsorption and regeneration experiments

MB solutions were prepared from the corresponding standard stock solutions by diluting with deionized water to different concentrations. MB solution was taken in Erlenmeyer flasks with fixed volume (50 mL). SCGG was added to the MB solutions in different amounts. The Erlenmeyer flasks were placed in a water-bathing constant temperature vibrator. The upper layer liquid was analyzed at a wavelength of 664 nm using a UV-visible spectrophotometer after a certain time. The removal rate (R) (1) and adsorption capacity (q_e) (2) were calculated as follows:

$$R = \frac{C_0 - C_e}{C_0} \times 100\% \quad (1)$$

$$q_e = \frac{(C_0 - C_e) \times V}{m} \quad (2)$$

where C_0 (mg L^{-1}) and C_e (mg L^{-1}) are the initial and equilibrium concentrations of the MB solutions, respectively; m (g) is the weight of the SCGG used; and V (L) is the volume of the MB solution.

The SCGG was desorbed using 0.1 mol L^{-1} HCl solution after saturated adsorption of MB. The Erlenmeyer flask that contained 0.1 mol L^{-1} HCl and saturated SCGG was placed in a water-bathing constant temperature vibrator for 3 h to complete desorption. Then, SCGG was filtered and washed three times to reach neutrality prior to the next adsorption experiment.

2.5. Deformation rate

The different weight of the balancing weight was put on gel balls to change their diameters, and a Vernier caliper was used to measure the average diameters.

2.6. Characterization

Atomic force microscopy (AFM, PicoPlus, Molecular Imaging, USA) was used to analyze the thickness of the samples in the tapping mode at a scanning rate of 0.5 Hz. Fourier transform infrared (FTIR) spectrum was obtained using a Fourier transform infrared spectrometer (iS10, Nicolet, USA). The spectra

were acquired in the wavenumber range from 4000 to 400 cm^{-1}. X-ray diffraction (XRD) patterns were obtained using an advance diffractometer (D/MAX2200, Rigaku, Japan) with Cu Kα radiation ($\lambda = 1.5418$ Å) operating at 40 kV and 30 mA. Samples were scanned in the range $5° < 2\theta < 60°$ with a scan interval of 0.02°. The morphology and structure of the samples were characterized *via* a scanning electron microscope (SEM, QUANTA200, FEI, Holland), and the samples were treated with spray gold. Frequently, the samples were covered using a vacuum cover system for the evaporation of metals. UV-vis spectra were acquired using a spectrophotometer (TU-1900, Beijing Purkinje General, China) in the scan range between 200 and 800 nm. A transmission electron microscope (JEM-2100, JEOL, Japan) was used to study the morphology of the samples at an accelerating voltage of 200 KV. Thermogravimetric analysis (TGA, Q50, TA instrument, USA) was used to detect the thermal stability under a N_2 atmosphere at the heating rate of 10 °C min^{-1} from 25 °C to 600 °C.

3. Results and discussion

3.1. Sample characteristics

The information about the size and thickness of the GO sheets was obtained *via* AFM. As shown in Fig. 1(a), the GO sheets exist as micrometer-sized planes, and the thickness of the GO flakes is very uniform, ranging from 1 to 2 nm, suggesting the complete exfoliation of GO sheets down to individual or bilayer sheets. The TEM image in Fig. 1(f) shows a good dispersion of GO nanosheets with some crinkles on the surface. The GO solution exhibited excellent water solubility and could retain its homogeneous state for a long time.

The image of MB adsorption on SCGG before and after is shown in Fig. 1(b). As seen from Fig. 1(b), SCGG has a uniform size and is faint yellow in color because of the presence of GO. However, after the adsorption of MB, SCGG turned dark blue-black.

The internal morphology of the SCGG is shown in Fig. 1(c–e). As shown in the figure, a honeycomb-like three-dimensional net structure can be clearly seen, and the pores of the SCGG are different. The structure not only increases the specific surface area of SCGG, but also increases the adsorption capacity of the active adsorptive sites, which is beneficial for the adsorption of the MB.

The FT-IR spectra of GO, SA, β-CD, SCGG-1 (before adsorption), and SCGG-2 (after adsorption) are shown in Fig. 2(a). The broad adsorption band at 3312 cm^{-1} is ascribed to the –OH stretching vibration of the hydroxyl group.[25] The band at 2925 cm^{-1} is assigned to the antisymmetric stretching vibrations of the methylene group. The peak appearing at 1731 cm^{-1} is associated with the –C=O stretching vibrations of the carbonyl and carboxylic groups. The absorption bands around 1600 cm^{-1} can be attributed to the asymmetric stretching vibrations of the COO– group.[26] The peak at 1418 cm^{-1} was assigned to C–OH. Moreover, the C–O–C and C–O stretching vibration peaks appeared at 1223 cm^{-1} and 1023 cm^{-1}, respectively. The presence of various oxygenous functional groups indicated that graphite was successfully oxidized. The abundant oxygenous functional groups make GO sheets strongly hydrophilic, which improve their solubility in water. These spectral results show that SCGG not only contains SA, β-CD, and GO, but also demonstrate the presence of composite reactions. In the spectra of SCGG-2, the peak at 1486 cm^{-1} was assigned to C=N; the stretching vibration peak of C–N is located at 881 cm^{-1}, and the stretching vibration peaks at 730–900 cm^{-1} can be attributed to the skeleton of benzene. Based on these results, it can be concluded that MB adsorption on SCGG has occurred.

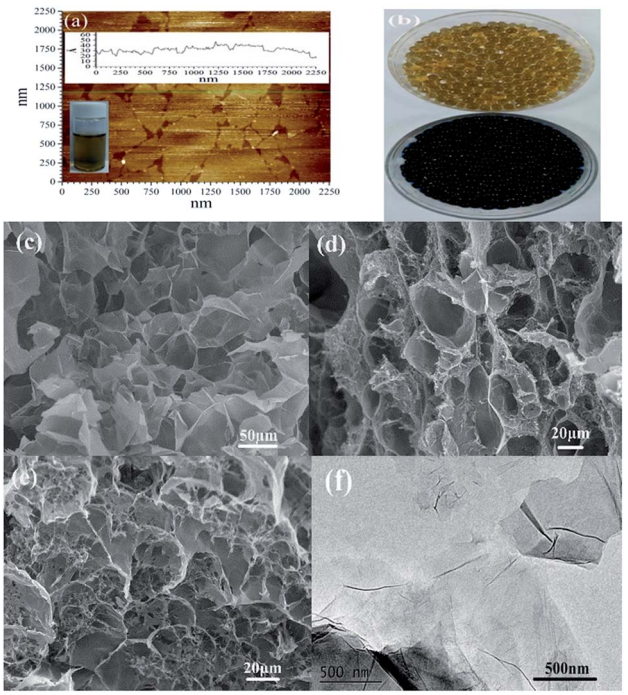

Fig. 1 The AFM image of GO (a), images obtained before and after adsorption (b), SEM images (c–e) of SCGG and TEM image of GO (f).

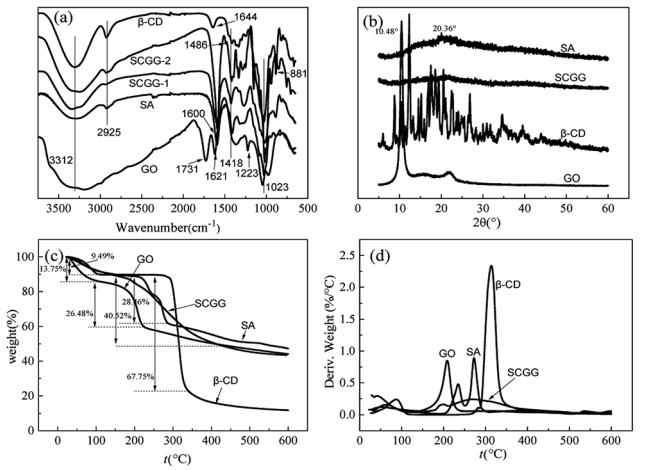

Fig. 2 FT-IR spectra (a), XRD patterns (b), TGA (c) and DTG (d) curves of GO, SA, β-CD, and SCGG.

XRD patterns of GO, SA, β-CD, and SCGG are in Fig. 2(b). The GO pattern showed an intense and sharp peak at 10.48°. According to the Bragg equation,[27] this peak corresponded to a *d*-spacing of 0.8441 nm, which confirms the synthesis of GO.[28] In the XRD spectrum of SA, the broad peak at 20.36° demonstrated the amorphous structure of SA. SA was usually semi-crystalline due to the strong interaction between alginate chains through intermolecular hydrogen bonding.[29] The XRD pattern of β-CD showed multiple diffraction peaks, which indicated that β-CD had a non-crystal structure. The SCGG pattern was similar to the SA pattern. This may be due to the low GO content in the SCGG. Because of the low content of GO in SCGG, the XRD spectrum of SCGG did not show a significant GO diffraction peak; moreover, more information was obtained, which indicated that the SCGG had an amorphous structure.

To determine the thermal stability, the mass–temperature relation was studied *via* TGA. TGA and DTG curves of GO, SA, β-CD, and SCGG are shown in Fig. 2(c and d). In the case of GO and β-CD, the first weight loss stage between 25 and 100 °C was associated with the evaporation of water adsorbed on the surface. With the increasing temperature, a major weight lost was observed from 100 to 225 °C, attributed to the thermal decompositions of oxygenous functional groups of GO.[30] The weight loss of β-CD reached 67.75% from 100 to 340 °C; this can be attributed to the decomposition of oxygenous functional groups and the hexatomic ring chains fractured.[31] The TGA curve trends of SA and SCGG were similar in the temperature range from 25 and 150 °C, which were assigned to adsorbed water on the surface. The temperature of the second weight loss stage reached 290 and 430 °C for SA and SCGG, respectively. The second degradation temperature was increased. The difference in temperature may be attributed to the egg-box structure formed due to ion exchange of Ca^{2+}. Thus, SCGG had high thermal stability.

3.2. Adsorption and regeneration studies

To choose a suitable dosage of adsorbent, different dosages of SCGG were added to 50 mL of 50 mg L^{-1} MB solutions. The results are shown in Fig. 3(a). The adsorption capacity for MB dyes on SCGG decreased from 214.32 mg g^{-1} to 133.24 mg g^{-1} with the increase in dosage from 0.5 to 1.0 g. The adsorption capacity decreased with the further increase in the amount of SCGG, whereas the removal rate increased with the increase in the amount of SCGG. This could be attributed to the increased surface area of the absorbent and availability of more active adsorptive sites with the increase in the amount of SCGG.[32] However, a further increase in the amount of the absorbent caused a decrease in the utilization rate of the SCGG active adsorption sites.[33] Thus, the 1.0 g amount of SCGG was considered for the next study.

H^+ concentration in solution is an important parameter that influences the adsorption behavior of dyes in an aqueous solution. It affects the surface charge of the adsorbent and the structure of the dyes.[34] The effects of the solution pH (from 4 to 10) on the adsorption are presented in Fig. 3(b). The adsorption capacity for MB dye on SCGG increased from 118.64 mg g^{-1} to 133.24 mg g^{-1} as the pH approached 7.0. Moreover, the removal rate of MB dye on SCGG increased from 75.67% to 84.98%. Thereafter, with the increase of solution pH, the removal rate and adsorption capacity showed a decreasing trend. As a cationic dye, MB exists in the aqueous solution in the form of cationic groups (MB^+). This could be explained on the basis of the H^+ concentration. When the pH was low, H^+ competed with MB for the active adsorptive sites on the SCGG.[35] With the increase of pH, the decrease of H^+ in solution was beneficial for the adsorption of MB on SCGG. The removal rate and adsorption capacity of SCGG for MB showed a decreasing tendency when the pH was more than 7. The mutual attraction between MB and OH^- affected the removal rate and adsorption capacity of SCGG for MB.

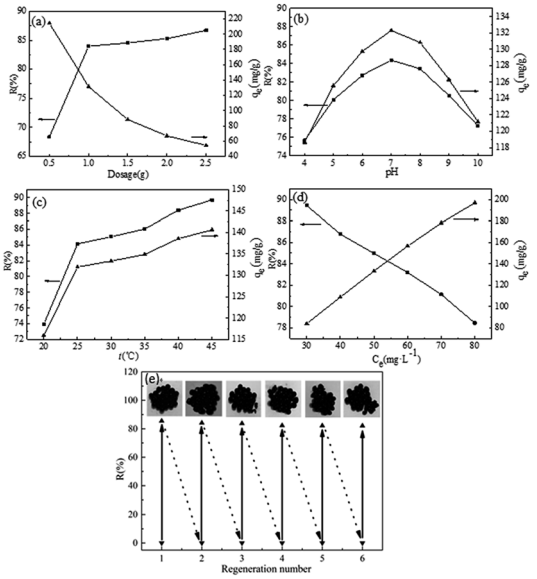

Fig. 3 Effects of adsorbent dose (a), solution pH (b), temperature (c), and initial MB concentration (d) on adsorption and the regeneration of SCGG (inset is the image of SCGG after adsorption) (e).

Temperature affects the diffusion capacity of the dye molecules and the viscosity of the solution. The diffusion capacity of the dye molecules was enhanced, and the solution viscosity decreased with the increase in temperature. Furthermore, the equilibrium capacity of the adsorbent for a particular adsorbate can be modified by changing the temperature. Effects of temperature on the adsorption are shown in Fig. 3(c). The removal rate and adsorption capacity of SCGG for MB showed an increasing trend with an increase in temperature. The abovementioned results indicated that the adsorption process was endothermic in nature. This could be attributed to the following facts: (I) as the temperature increased, the diffusion capacity of the dye molecules enhanced, and the diffusion of MB into the active adsorptive sites became much easier[36] and (II) the viscosity of the solution decreased with an increase in temperature.

MB adsorption is significantly influenced by the initial concentration of MB in the aqueous solution. The effect of the initial concentration of MB ranging from 30 to 80 mg L^{-1} on the

SCGG adsorption was investigated, and the results are presented in Fig. 3(d). The adsorption capacity of MB dye gradually increased when the concentration increased. On the contrary, the removal rate of the MB dye gradually decreased when the concentration increased. Owing to the number of MB molecules was less to the active adsorptive sites when the concentration is low.[37] Therefore, the removal rate was high. The effective chance of collision between MB and SCGG was increased and the mass transfer resistance decreased with the increase in the initial concentration of MB.[38] Therefore, the adsorption capacity of SCGG for MB gradually increased. However, due to the saturation of SCGG active adsorption sites, low removal rate of MB was observed.

The regeneration ability of an adsorbent is an important factor to evaluate the practical application of the adsorbent. The breakage rate of SCGG in the adsorption–desorption eqn (3) is expressed as follow:

$$B = \frac{N_b}{N_a} \times 100\% \quad (3)$$

where N_b is the breakage number of SCGG and N_a is the total number of SCGG.

SCGG-0%, SCGG-5%, and SCGG-10% represent SCGG containing 0, 5, and 10% GO, respectively. From Table 1, it was observed that the deformation rate of SCGG decreased with the increase in the GO content. This result suggested that the mechanical property of SCGG increased with the increase in the content of GO.

The cycles of adsorption–desorption experiments were carried out, as shown in Fig. 3(e). The removal rate of MB decreased for each new cycle after desorption for six cycles. After six cycles, the removal rate of MB on SCGG was still above 82% and the adsorption capacity was more than 130.68 mg g^{-1}, which demonstrated that SCGG could be effectively regenerated and reused for the adsorption of MB with good adsorption performance. The breakage rates of SCGG-0% in the regeneration recycle were 0, 4, 8, 16, 24, and 32%. The breakage rates of SCGG in the regeneration recycle were 0, 0, 4, 12, 16, and 20% because the spherical structure of SCGG is gradually destroyed during the desorption process of shock. The mechanical property of the SCGG was enhanced due to the addition of GO; although the spherical structure SCGG was damaged during the process of desorption, it did not affect the adsorption properties. The regeneration removal rates of MB were 84.98, 84.14, 83.76, 82.32, 82.15, and 82.08% in six cycles. The adsorption capacity and regeneration number of MB on SCGG was considerable as compared to those of other biological adsorbents reported in the literature, as shown in Table 2. Scheme 1 illustrates the probable reaction between SCGG and MB.[45] The SA and β-CD were biodegradable, which have a good prospect.

Table 2 Comparison of adsorption capacities and regeneration number of various adsorbents for MB removal

Adsorbent	q_e (mg g^{-1})	Regeneration number	Sources
Modified ball clay and chitosan composite	26.93	5	39
Potato leaves powder	52.60	3	40
Magnetic chitosan and GO	95.16	4	41
Starch–humic composite hydrogel	110.00	5	42
GO–SA	123.10	—	43
Citrus limetta peel	227.30	—	44
SCGG	132.09	6	This work

3.3. Study of the adsorption isotherms

The interaction model between SCGG and MB could be described using the adsorption isotherms. Adsorption isotherms were obtained at different temperatures. The adsorption isotherm reflected the linear relationship between the adsorption capacity and equilibrium concentration of the

Table 1 Mechanical property and breakage rate of SCGG with different contents of GO

	Weight (g)	Length (cm)	Diameter (cm)	Deformation rate (%)	Breakage rate in 5 cycles (%)	
SCGG-0%	0	8.58	0.2860	0	1	0
	10	8.76	0.2920	2.0979	2	4
	20	8.94	0.2980	4.1958	3	8
	50	9.13	0.3043	6.4103	4	16
	100	9.25	0.3083	7.8089	5	24
SCGG-5%	0	8.64	0.2880	0	1	0
	10	8.71	0.2903	0.8102	2	0
	20	8.85	0.2950	2.4306	3	4
	50	8.96	0.2987	3.7037	4	8
	100	9.04	0.3013	4.6296	5	16
SCGG-10%	0	8.05	0.2683	0	1	0
	10	8.11	0.2703	0.7453	2	0
	20	8.14	0.2713	1.1180	3	0
	50	8.18	0.2727	1.6149	4	4
	100	8.25	0.2750	2.4845	5	12

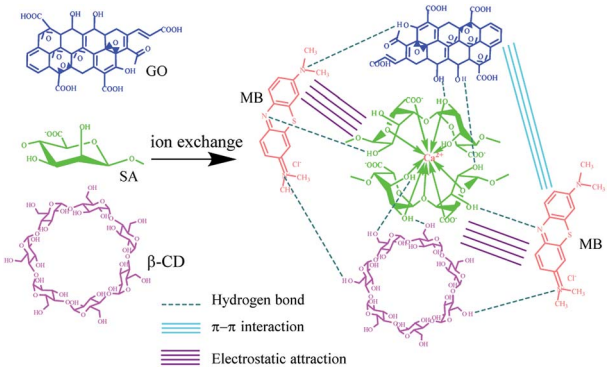

Scheme 1 Schematic of the probable reaction between SCGG and MB.

solution at a certain temperature. The adsorption isotherm model can be further used to study the mechanism of adsorption. The commonly used model, including Langmuir (4)[46] and Freundlich (5)[47] model, is as follows:

$$\frac{C_e}{q_e} = \frac{C_e}{q_{max}} + \frac{1}{q_{max}k_L} \quad (4)$$

$$\ln q_e = \ln k_F + \frac{1}{n}\ln C_e \quad (5)$$

where C_e (mg L^{-1}) is the equilibrium concentration of the MB solution; q_e (mg g^{-1}) is the amount of MB adsorbed on the absorbent; q_{max} (mg g^{-1}) is the maximum amount of MB adsorbed on the absorbent; k_L (L mg^{-1}) is the Langmuir equilibrium adsorption constant; k_F is the Freundlich characteristic adsorption constant; and n is the constant.

The experimental data were analyzed using the Langmuir model and Freundlich model, as shown in Fig. 4(a–c). The fitting parameters are listed in Table 3. As observed in the from Table 3, the correlation coefficient of the Freundlich model (R^2 > 0.99) was greater than that of the Langmuir model (R^2 > 0.98) at the same temperature, which indicated that the experimental data fitted well with the Freundlich model. Furthermore, the essential feature of the Langmuir isotherm model is a separation factor R_L (6), belonging to a dimensionless constant, which is defined by

$$R_L = \frac{1}{1 + C_0 k_L} \quad (6)$$

where C_0 is the initial MB concentration and k_L is the Langmuir equilibrium constant. The values of R_L indicates the tendency of the adsorption process, which can be unfavorable (R_L > 1), linear (R_L = 1), favorable (0 < R_L < 1), irreversible (R_L = 0), and unfavorable (R_L < 0). In this study, all the R_L values were 0.1491, 0.1514, and 0.1559 corresponding to 25, 35, and 45 °C, respectively, which indicated that the adsorption of MB on SCGG was favorable.[48] The values of n in the range of 1–10 suggested favorable adsorption for MB on the SCGG.[49] This may be attributed to the large specific surface area of GO and the rich functional groups present in SCGG.

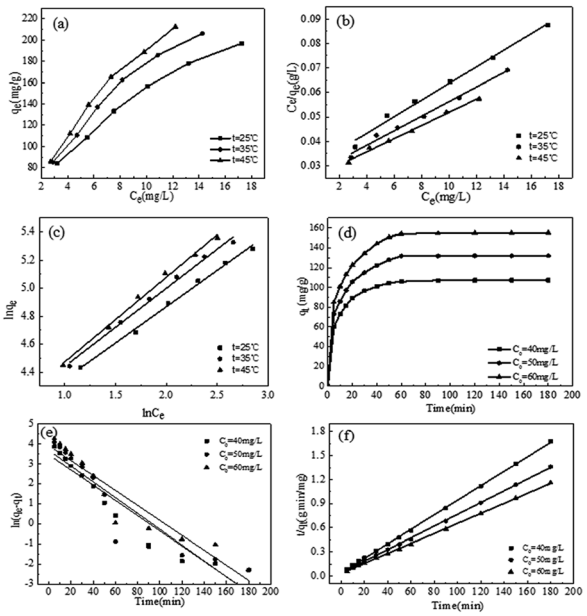

Fig. 4 Adsorption isotherms of MB on SCGG (a), adsorption data obtained and fitted with different models: Langmuir (b), Freundlich (c) at different temperatures, kinetic curves of different initial concentrations of MB (d), and adsorption kinetics data of MB onto SCGG fitted with the pseudo-first-order model (e) and the pseudo-second-order model (f).

3.4. Study of the adsorption kinetics

To investigate the mechanism and kinetics for the adsorption of MB on SCGG, adsorption experiments were carried out using three different concentrations of MB (20, 30, 40 mg L^{-1}), and the results are shown in Fig. 4(d–f). As observed from Fig. 4(d), with the extension of adsorption time, the adsorption of MB on SCGG was a fast process in the initial 20 min, the adsorption rate slowed down between 20 and 60 min, and the adsorption process reached a balance at 120 min. This can be attributed to the high concentration of MB in the solution and more active adsorption sites in the initial stage of adsorption; moreover, the mass transfer driving force was large. Therefore, the adsorption rate of MB on SCGG was fast. As adsorption progressed, the concentration of MB decreased and the active adsorption sites were gradually saturated; thus, the adsorption rate became slow. As the MB molecules on the surface of SCGG entered the internal areas of SCGG *via* diffusion, the adsorption capacity slowly increased and eventually reached equilibrium. Therefore, the adsorption time required for the adsorption capacity to reach equilibrium was about 180 min.

Adsorption kinetics is used to study the linear relationship between the adsorption capacity and time. The commonly used models include the pseudo-first-order kinetic eqn (7)[50] and the pseudo-second-order kinetic eqn (8).[4] They are calculated using the following equations

$$\ln(q_e - q_t) = \ln q_e - k_1 t \quad (7)$$

$$\frac{t}{q_t} = \frac{1}{k_2 q_e^2} + \frac{t}{q_e} \quad (8)$$

Table 3 The isothermal adsorption parameters and thermodynamic parameters of MB adsorption on SCGG at different temperatures

	Langmuir			Freundlich					
T (°C)	k_L (L mg)	q_{max} (mg g^{-1})	R^2	k_F	n	R^2	ΔG (kJ mol^{-1})	ΔH (kJ mol^{-1})	ΔS (J (mol^{-1} K^{-1}))
25	0.1141	294.9853	0.9881	46.1455	1.9286	0.9943	−6.5560		
35	0.1121	336.7003	0.9883	48.6280	1.7918	0.9925	−7.3425	16.8798	78.6438
45	0.1083	370.3704	0.9824	47.4796	1.6525	0.9935	−8.1289		

Table 4 Kinetic parameters of different initial concentrations of MB[a]

	Pseudo-first-order kinetic equation				Pseudo-second-order kinetic equation			
C_0 (mg L^{-1})	k_1 (min^{-1})	$q_{e,cal}$ (mg g^{-1})	$q_{e,exp}$ (mg g^{-1})	R^2	k_2 (g mg^{-1} min^{-1})	$q_{e,cal}$ (mg g^{-1})	$q_{e,exp}$ (mg g^{-1})	R^2
40	0.0380	31.3044	107.3619	0.9146	0.0022	110.4972	107.3619	0.9937
50	0.0394	39.1703	133.2428	0.8455	0.0015	136.6120	133.2428	0.9895
60	0.0373	49.3861	155.1953	0.9014	0.0013	160.5136	155.1953	0.9876

[a] $q_{e,cal}$ is the calculated equilibrium adsorption capacity and $q_{e,exp}$ is the experimental equilibrium adsorption capacity.

where q_e (mg g^{-1}) is the equilibrium adsorption capacity; q_t (mg g^{-1}) is the adsorption capacity at t; k_1 (min^{-1}) is the pseudo-first-order kinetic rate constant; and k_2 (g (mg^{-1} min^{-1})) is the pseudo-second-order kinetic constant. The kinetic equation and adsorption data are listed in Table 4.

The experimental data were fitted with the pseudo-first-order kinetic equation and the pseudo-second-order kinetic equation. The fitting results are shown in Table 4. As observed from Table 4, when the initial concentration of MB was 40 mg L^{-1}, there were significant differences between the equilibrium adsorption values calculated by the pseudo-first-order kinetic equation (31.3044 mg g^{-1}) and those calculated *via* the experiment (107.3619 mg g^{-1}). On the contrary, the equilibrium adsorption capacity calculated by the pseudo-second-order kinetic equation (110.4972 mg g^{-1}) was closer to the experimental value (107.3619 mg g^{-1}). The results of the other two concentrations were consistent with this rule. Furthermore, the correlation coefficients of the pseudo-second-order kinetic equation (R^2 > 0.98) were higher than those of the pseudo-first-order kinetic equation (R^2 > 0.84). Therefore, the experimental data were well represented by the pseudo-second-order kinetic equation.

3.5. Study of the adsorption thermodynamic

To further study the influence of temperature on the adsorption of MB and explore the thermodynamic changes of the adsorption process, adsorption experiments were carried out at 298, 308, and 318 K. The adsorption equilibrium constant (9) and thermodynamic eqn (10) and (11) are expressed as follows:

$$K_d = \frac{q_e}{C_e} \quad (9)$$

$$\ln K_d = -\frac{\Delta H}{RT} + \frac{\Delta S}{R} \quad (10)$$

$$\Delta G = \Delta H - T\Delta S \quad (11)$$

where K_d (L g^{-1}) is the distribution coefficient; q_e (mg g^{-1}) is the adsorption capacity at equilibrium; C_e (mg L^{-1}) is the concentration of the MB solution at equilibrium; R (8.314 J (mol^{-1} K^{-1})) is the ideal gas constant; ΔH (kJ mol^{-1}) is the standard change in enthalpy; ΔS (J (mol^{-1} K^{-1})) is the standard change in entropy; and ΔG (kJ mol^{-1}) is the Gibbs free energy change in a given process.

Moreover, thermodynamic parameters were calculated according to eqn (9)–(11), and the results are shown in Table 3. ΔG values were calculated to be −6.5560, −7.3425, and −8.1289 kJ mol^{-1} at 298, 308, and 318 K, respectively. Negative ΔG values indicated spontaneous adsorption.[51] Furthermore, ΔG values decreases with the increase in temperature, which indicate that better adsorption performance can be obtained when the temperature is higher. The positive values of ΔH confirmed the endothermic nature of the overall adsorption process.[52] Finally, the positive value of ΔS suggested an increased randomness at the solid–liquid interface during the adsorption of MB on SCGG.[53]

4. Conclusion

In the present study, highly water soluble GO was synthetized *via* a modified Hummers method. A novel SA-based adsorbent (SCGG) was successfully prepared, and the removal of MB in an aqueous solution was studied using SCGG. The equilibrium data were well-modeled by the Freundlich isotherm model. The kinetic study showed that the adsorption process followed the pseudo-second-order kinetic model. The thermodynamic data indicated that the adsorption process was spontaneous and endothermic in nature. Moreover, the mechanical property of SCGG was improved, the deformation rate was decreased, and the breakage rate was decreased due to the addition of GO. The

removal rate of MB was significant after six cycles. Based on the above mentioned experimental results and the advantages, such as cost-effectiveness, biodegradability, ease of operation, and high efficiency, of SCGG, it can be concluded that SCGG has great potential applications in industrial wastewater treatment and environmental protection.

Acknowledgements

This study was funded by the National Natural Science Foundation of China (No. 31670592), the Central University Basic Scientific Research Project of China (No. 2572017EB03), and the Research Funds for the Returned People of Heilongjiang Province (No. LC2016008).

Notes and references

1 M. Bhaumik, R. McCrindle and A. Maity, *Chem. Eng. J.*, 2013, **228**, 506–515.
2 H. Mittal, V. Kumar, Saruchi and S. S. Ray, *Int. J. Biol. Macromol.*, 2016, **89**, 1–11.
3 V. K. Gupta and Suhas, *J. Environ. Manage.*, 2009, **90**, 2313–2342.
4 N. K. Goel, V. Kumar, N. Misra and L. Varshney, *Carbohydr. Polym.*, 2015, **132**, 444–451.
5 Y. Li, Q. Du, T. Liu, Y. Qi, P. Zhang, Z. Wang and Y. Xia, *Appl. Surf. Sci.*, 2011, **257**, 10621–10627.
6 B. H. Hameed and A. A. Ahmad, *J. Hazard. Mater.*, 2009, **164**, 870–875.
7 D. Mahanta, G. Madras, S. Radhakrishnan and S. Patil, *J. Phys. Chem. B*, 2009, **113**, 2293–2299.
8 Y. Yao, F. Xu, M. Chen, Z. Xu and Z. Zhu, *Bioresour. Technol.*, 2010, **101**, 3040–3046.
9 B. H. Hameed, A. T. M. Din and A. L. Ahmad, *J. Hazard. Mater.*, 2007, **141**, 819–825.
10 O. Hamdaoui, *J. Hazard. Mater.*, 2006, **135**, 264–273.
11 E. Alver, M. Bulut, A. Ü. Metin and H. Çiftçi, *Spectrochim. Acta, Part A*, 2017, **171**, 132–138.
12 N. E. Mousa, C. M. Simonescu, R.-E. Pătescu, C. Onose, C. Tardei, D. C. Culiță, O. Oprea, D. Patroi and V. Lavric, *React. Funct. Polym.*, 2016, **109**, 137–150.
13 K. Shweta and H. Jha, *Biotechnol. Rep.*, 2015, **7**, 95–106.
14 X. Zhu, L. Bao, Y. Wei, J. Ma and Y. Kong, *Int. J. Biol. Macromol.*, 2016, **91**, 409–415.
15 S. N. Pawar and K. J. Edgar, *Biomaterials*, 2012, **33**, 3279–3305.
16 L. Sun and B. Fugetsu, *Chem. Eng. J.*, 2014, **240**, 565–573.
17 S. Zhang, F. Xu, Y. Wang, W. Zhang, X. Peng and F. Pepe, *Chem. Eng. J.*, 2013, **234**, 33–42.
18 G. Jie, Z. Kongyin, Z. Xinxin, C. Zhijiang, C. Min, C. Tian and W. Junfu, *Mater. Lett.*, 2015, **157**, 112–115.
19 C. Chang, B. Duan and L. Zhang, *Polymer*, 2009, **50**, 5467–5473.
20 Y. He, N. Zhang, Q. Gong, H. Qiu, W. Wang, Y. Liu and J. Gao, *Carbohydr. Polym.*, 2012, **88**, 1100–1108.
21 W. Peng, H. Li, Y. Liu and S. Song, *J. Mol. Liq.*, 2016, **221**, 82–87.
22 Y. Pan, T. Wu, H. Bao and L. Li, *Carbohydr. Polym.*, 2011, **83**, 1908–1915.
23 M.-j. Li, C.-m. Liu, Y.-b. Xie, H.-b. Cao, H. Zhao and Y. Zhang, *Carbon*, 2014, **66**, 302–311.
24 W. S. Hummers and R. E. Offeman, *J. Am. Chem. Soc.*, 1958, **80**, 1339.
25 Y. Zhang, Y. Liu, X. Wang, Z. Sun, J. Ma, T. Wu, F. Xing and J. Gao, *Carbohydr. Polym.*, 2014, **101**, 392–400.
26 M. M. Lakouraj, F. Mojerlou and E. N. Zare, *Carbohydr. Polym.*, 2014, **106**, 34–41.
27 W. H. Bragg and W. L. Bragg, *Proc. R. Soc. London, Ser. A*, 1913, **88**, 428–438.
28 T.-T. Wu and J.-M. Ting, *Surf. Coat. Technol.*, 2013, **231**, 487–491.
29 S. Thakur, S. Pandey and O. A. Arotiba, *Carbohydr. Polym.*, 2016, **153**, 34–46.
30 G. Jiang, Z. Lin, C. Chen, L. Zhu, Q. Chang, N. Wang, W. Wei and H. Tang, *Carbon*, 2011, **49**, 2693–2701.
31 A. Mahmood, M. Ahmad, R. M. Sarfraz and M. U. Minhas, *J. Drug Delivery Sci. Technol.*, 2016, **36**, 75–88.
32 H. Ren, Z. Gao, D. Wu, J. Jiang, Y. Sun and C. Luo, *Carbohydr. Polym.*, 2016, **137**, 402–409.
33 X. Sun, J. H. Chen, Z. Su, Y. Huang and X. Dong, *Chem. Eng. J.*, 2016, **290**, 1–11.
34 A. Sigdel, J. Park, H. Kwak and P.-K. Park, *J. Ind. Eng. Chem.*, 2016, **35**, 277–286.
35 R. Ahmad, *J. Hazard. Mater.*, 2009, **171**, 767–773.
36 V. Srivastava, C. H. Weng, V. K. Singh and Y. C. Sharma, *J. Chem. Eng. Data*, 2011, **56**, 1414–1422.
37 C. Cheng, L. Ma, J. Ren, L. Li, G. Zhang, Q. Yang and C. Zhao, *Chem. Eng. J.*, 2011, **171**, 1132–1142.
38 A. Benhouria, M. A. Islam, H. Zaghouane-Boudiaf, M. Boutahala and B. H. Hameed, *Chem. Eng. J.*, 2015, **270**, 621–630.
39 M. Auta and B. H. Hameed, *Chem. Eng. J.*, 2014, **237**, 352–361.
40 N. Gupta, A. K. Kushwaha and M. C. Chattopadhyaya, *Arabian J. Chem.*, 2016, **9**(1), S707–S716.
41 L. Fan, C. Luo, X. Li, F. Lu, H. Qiu and M. Sun, *J. Hazard. Mater.*, 2012, **215–216**, 272–279.
42 R. Chen, Y. Zhang, L. Shen, X. Wang, J. Chen, A. Ma and W. Jiang, *Chem. Eng. J.*, 2015, **268**, 348–355.
43 T. Ma, P. R. Chang, P. Zheng, F. Zhao and X. Ma, *Chem. Eng. J.*, 2014, **240**, 595–600.
44 S. Shakoor and A. Nasar, *J. Taiwan Inst. Chem. Eng.*, 2016, **66**, 154–163.
45 M. Heidarizad and S. S. Şengör, *J. Mol. Liq.*, 2016, **224**, 607–617.
46 G. Zhang, L. Yi, H. Deng and P. Sun, *J. Environ. Sci.*, 2014, **26**, 1203–1211.
47 J.-H. Deng, X.-R. Zhang, G.-M. Zeng, J.-L. Gong, Q.-Y. Niu and J. Liang, *Chem. Eng. J.*, 2013, **226**, 189–200.
48 L.-g. Yan, K. Yang, R.-r. Shan, T. Yan, J. Wei, S.-j. Yu, H.-q. Yu and B. Du, *J. Colloid Interface Sci.*, 2015, **448**, 508–516.
49 Y. Li, Q. Du, T. Liu, J. Sun, Y. Wang, S. Wu, Z. Wang, Y. Xia and L. Xia, *Carbohydr. Polym.*, 2013, **95**, 501–507.

50 P. Sharma, B. K. Saikia and M. R. Das, *Colloids Surf., A*, 2014, **457**, 125–133.
51 A. N. Fernandes, C. A. P. Almeida, N. A. Debacher and M. M. d. S. Sierra, *J. Mol. Struct.*, 2010, **982**, 62–65.
52 L. Ai, C. Zhang and Z. Chen, *J. Hazard. Mater.*, 2011, **192**, 1515–1524.
53 S. Shrestha, G. Son, S. H. Lee and T. G. Lee, *Chemosphere*, 2013, **92**, 1053–1061.